Heat transfer model for the simulation of spindle heating and expansion inside a multiphase screw pump

Dipl.-Ing. (FH) Klaus Räbiger
Prof. Dr. T.M.A. Maksoud
Prof. Dr. John Ward

University of Glamorgan
School of Technology
Wales, UK

Prof. Dr. G. Hausmann

Georg-Simon-Ohm Fachhochschule Nürnberg
Fachbereich Maschinenbau und
Versorgungstechnik

Abstract

The multiphase application of screw pumps, especially at high pressures and gas volume fractions implicates thermal loads for the solid components of the pump. For the evaluation of these loads and their consequences, a finite volume heat transfer model for the screws, as the main parts of a screw pump, was developed to describe and simulate the transient and 3-dimensional heat transfer process. The time-dependent heat transfer is mainly influenced by convection and thus by the rotational speed of the screws and by the temperature distribution of the multiphase fluid along the screw surface.

Key words : screw pump - heat transfer - finite volume - convection - heat conduction

ISSN 1616-0762 Sonderdruck Schriftenreihe der Georg-Simon-Ohm-Fachhochschule Nürnberg Nr. 33, November 2005

1. Introduction

The type of pump, whose main component will be theoretically investigated in this paper, is a twin screw pump, which can be used for multiphase operations. A screw pump is a particular type of rotary displacement pump, in which a number of screws rotate inside a cylindrical housing. The geometry and rotation of the screws generate a series of closed chambers, which transport the fluid from the low pressure inlet to the high pressure outlet, see figure 1.1.

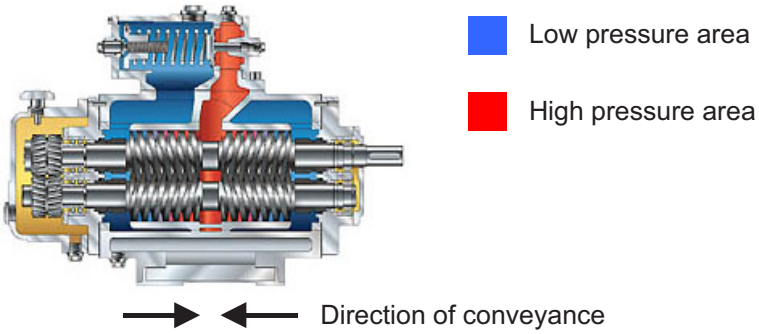

Figure 1.1 : Multiphase screw pump

Previous investigations of multiphase screw pumps have largely been concerned with the general pumping behaviour of these systems [1]. Moreover these studies have been restricted to medium sized pumps, in which the driving power and gas concentrations are relatively modest. In these situations the heat capacity and density of the gas-liquid mixture is dominated by the liquid phase so that the pumping process is essentially isothermal and thermodynamic effects can be neglected [2] and [3]. In the case of pumping multiphase mixtures with high gas volume fractions in combination with high pressure differences over a longer period, the remaining amount of liquid is not able to absorb the compression heat of the compressible gas phase. Also at medium mean gas volume fractions, it could be possible that the pump have to convey a mixture with a much higher gas content for a certain time, so that the above mentioned disregard cannot be justified for this extended range of multiphase application. The leakage flows through the different gaps at a gas volume fraction of 100 % were investigated numerically [4], to determine the compressibility and acceleration effects of the gas phase inside the gaps.

There are existing two new models [5] and [6], which include the thermodynamic effects by establishing mass and energy balance equations for the fluid flow through each chamber. Also the heat transfer effects inside the screw and the housing were investigated, [5]. But, no heat transfer model for the screws can be found in literature, which deals with the heat transfer including the tangential temperature gradient concerning the whole screw package including the shafts, see figure 1.2. There is a need for a model that can predict the resulting thermal expansion of the screw and the influence on the flow inside the perimeter and the radial gap by the changing of the gap-defining surfaces.

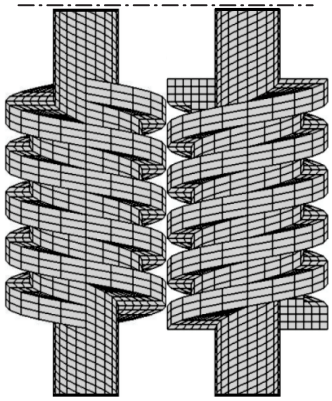

Figure 1.2 : A pair of meshing screws (taken apart)

Due to the lack of such a model and to prevent the ill effect of a conveyance break off due to a screw blockage inside the housing as a result of severe thermal effects, it is necessary to develop a new transient numerical heat transfer model for the whole screw.

2. Fundamentals of heat transfer

Heat conduction problems of several kinds are described by the following partial differential equation

$$\frac{\partial T}{\partial t} = a \cdot \left(\frac{\partial^2 T}{\partial x^2} + \frac{\partial^2 T}{\partial y^2} + \frac{\partial^2 T}{\partial z^2} \right) \pm \frac{\dot{q}}{\rho \cdot c_p} \qquad \text{(parabolic PDE)} \qquad (2.1)$$

For steady-state calculations without any heat sources and sinks the expression can be reduced to

$$\frac{\partial^2 T}{\partial x^2} + \frac{\partial^2 T}{\partial y^2} + \frac{\partial^2 T}{\partial z^2} = 0 \qquad \text{(elliptic PDE)} \qquad (2.2)$$

By introducing, besides the pure heat conduction and the consideration of heat sources and sinks, also the convection on the outer surface of a body, an energy balance equation can be introduced.

$$\frac{\partial Q_{cell}}{\partial t} = \sum_{n=1}^{6} \left(\pm \dot{q}_{conduction} \cdot A \right) + \sum_{n=1}^{6} \left(\pm \dot{q}_{convection} \cdot A \right) \pm \dot{Q}_{sink/source} \qquad (2.3)$$

with $$Q_{cell} = c_{cell} \cdot \rho_{cell} \cdot V_{cell} \cdot T_{cell} \qquad (2.4)$$

$$\dot{q}_{conduction} = -k \cdot \frac{\partial T}{\partial x_i} \qquad \text{(Fourier's law of heat conduction)} \qquad (2.5)$$

$$\dot{q}_{convection} = -h \cdot \left(T_{\infty} - T_{surface} \right) \qquad (2.6)$$

As a consequence of this, the temporal change of energy of a certain control volume is dependent on the heat fluxes in or out of this volume and possible heat sources and sinks inside this volume. Whereas the thermal conductivity is a property of the material, the convective heat transfer coefficient is a function of the flow and fluid condition around the surface of the body. In the case of the screw of a multiphase pump, it is assumed as a homogeneous equilibrium gas-liquid mixture, which is enclosed by the still-standing housing and three moving walls - two chamber flanks and one chamber ground. The calculation procedure, [7] [8] and [9], for determining the corresponding Nusselt number or the convective heat transfer coefficient, will be explained sequentially below.

Important non-dimensional parameters

Reynolds number $$Re = \frac{u_{\varphi} \cdot d_h \cdot \rho_H}{\mu_H} \qquad (2.7)$$

Prandtl number $$Pr = \frac{\mu_H \cdot c_{p,H}}{k_H} \qquad (2.8)$$

Nusselt number $$Nu = \frac{h \cdot d_h}{k_H} \qquad (2.9)$$

with $d_h = \pi \cdot 2 \cdot r_{cell\ position}$ (2.10) and $u_\varphi = \frac{2 \cdot \pi \cdot n}{60} \cdot r_{cell\ position}$ (2.11)

Mixture fluid properties (homogeneous equilibrium formulation)

mass fraction $$x = \frac{\alpha \cdot \rho_G}{(1-\alpha) \cdot \rho_L + \alpha \cdot \rho_G} \quad (2.12)$$

homogeneous density $$\rho_H = (1-\alpha) \cdot \rho_L + \alpha \cdot \rho_G \quad (2.13)$$

homogeneous dynamic viscosity $$\mu_H = (1-\alpha) \cdot \mu_L + \alpha \cdot \mu_G \quad (2.14)$$

homogeneous thermal conductivity $$k_H = (1-\alpha) \cdot k_L + \alpha \cdot k_G \quad (2.15)$$

homogeneous specific heat capacity $$c_{p,H} = (1-x) \cdot c_L + x \cdot c_{p,G} \quad (2.16)$$

Nusselt numbers for a flat plate in parallel flow

for laminar flows $Re < 6 \cdot 10^4$ and $0.6 < Pr < 10$

$$Nu = 0.332 \cdot Re^{1/2} \cdot Pr^{1/3} \quad (2.17)$$

for turbulent flows $5 \cdot 10^5 < Re < 10^7$ and $0.6 < Pr < 60$

$$Nu = 0.0296 \cdot Re^{4/5} \cdot Pr^{1/3} \quad \text{(Chilton \& Colburn)} \quad (2.18)$$

3. Finite volume method

The governing partial differential equation for the transient temperature field without any heat sources and sinks follows to

$$\frac{\partial T}{\partial t} = \frac{k_S}{c_S \cdot \rho_S} \cdot \left[\frac{\partial}{\partial x}\left(\frac{\partial T}{\partial x}\right) + \frac{\partial}{\partial y}\left(\frac{\partial T}{\partial y}\right) + \frac{\partial}{\partial z}\left(\frac{\partial T}{\partial z}\right) \right] \quad (3.1)$$

The finite volume method is a very efficient calculation method in the field of numerical heat transfer and computational fluid dynamics and is characterised as having a high accuracy compared to finite element method (FEM) and by a higher flexibility compared to the finite difference method (FDM).

The finite volume approach, [10] [11] and [12], is to integrate the derivative terms in the heat conduction equation with respect to the three space coordinates over the whole finite volume and then transform the results with the divergence theorem by Gauss.

Integration of the heat transfer equation

$$c_S \cdot \rho_S \cdot \iiint_V \left(\frac{\partial}{\partial t} I \right) dV + \iiint_V \left(\frac{\partial}{\partial x} J \right) dV + \iiint_V \left(\frac{\partial}{\partial y} K \right) dV + \iiint_V \left(\frac{\partial}{\partial z} L \right) dV = 0 \quad (3.2)$$

with the transient parameter $I = T$ (3.3)

and the heat flux densities

$$J = -k_S \cdot \frac{\partial T}{\partial x} \quad (3.4) \qquad K = -k_S \cdot \frac{\partial T}{\partial y} \quad (3.5) \qquad L = -k_S \cdot \frac{\partial T}{\partial z} \quad (3.6)$$

Notice : The equations 3.4 to 3.6 are only valid in the case of heat conduction, for example in the interior of the body. If the cell belongs to the surface of the screw, were convection can occur, other formulations for the heat flux densities must be used.

$$J, K, L = -h \cdot \left(T_{fluid} - T_{surface}\right) \quad (3.7)$$

Further details can be found below in the section of the applied boundary conditions.

Divergence theorem by Gauss

$$\iiint_V divF \, dV = \oiint_A F \, d\boldsymbol{A} = \oiint_A \left(F \cdot \boldsymbol{n}\right) dA \quad (3.8)$$

$$\boldsymbol{A}_l = \boldsymbol{n}_l \cdot A_l \quad (3.9)$$

Resulting equation (formulation for each cell of the whole domain)

$$c_S \cdot \rho_S \cdot \frac{d}{dt} I_{i,j,k} \cdot V_{i,j,k} + \sum_{m=1}^{3} \sum_{l=1}^{6} \left(F_{m,l} \cdot A_{m,l}\right)_{i,j,k} = 0 \quad (3.10)$$

with m = 1 ... 3 for each derivative in the three coordinate directions
l = 1 ... 6 for each face of the cell, here with a cuboid's shape

The resulting equation 3.10 is already formulated for 3-dimensional finite volume cells, which will be generated by a structured discretisation of the whole solid domain. As an example, a single cell with all notations can be seen below in figure 3.1.

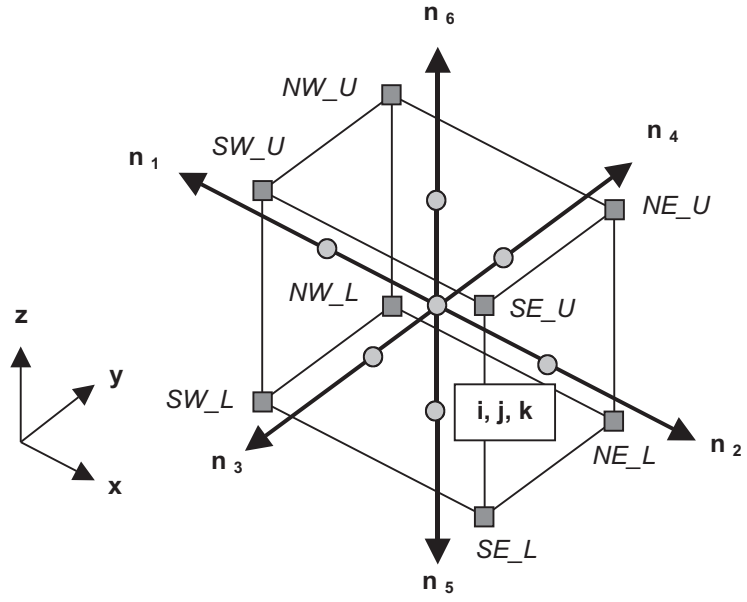

Figure 3.1 : 3-dimensional finite volume cell

The following form of equation 3.10 allows their direct use for the numerical calculation.

$$\frac{d}{dt} I_{i,j,k} = -\frac{1}{c_S \cdot \rho_S \cdot V_{i,j,k}} \cdot \begin{bmatrix} (J_1 \cdot A_{11}) + (J_2 \cdot A_{12}) + (J_3 \cdot A_{13}) + \\ (J_4 \cdot A_{14}) + (J_5 \cdot A_{15}) + (J_6 \cdot A_{16}) + \\ (K_1 \cdot A_{21}) + (K_2 \cdot A_{22}) + (K_3 \cdot A_{23}) + \\ (K_4 \cdot A_{24}) + (K_5 \cdot A_{25}) + (K_6 \cdot A_{26}) + \\ (L_1 \cdot A_{31}) + (L_2 \cdot A_{32}) + (L_3 \cdot A_{33}) + \\ (L_4 \cdot A_{34}) + (L_5 \cdot A_{35}) + (L_6 \cdot A_{36}) \end{bmatrix} \tag{3.11}$$

In the above expression 3.11, the parameter *I* is defined by the heat condition in the centre of the cell (cell-centred formulation). The parameters *J*, *K* and *L* are calculated against it in the middle of the six cell faces A_1 to A_6 by averaged state values of two neighbouring cells in the case of heat conduction or will be replaced by definite heat flux densities.

4. Time-stepping method

The time stepping method, which was chosen for this transient finite volume heat transfer model is a fourth-order Runge-Kutta scheme, [12], (fourth-order accuracy in time).

$$I_{i,j,k}^{(0)} = I_{i,j,k}^{(n)} \tag{4.1}$$

$$I_{i,j,k}^{(1)} = I_{i,j,k}^{(0)} - \alpha_1 \cdot \frac{\Delta t}{c_S \cdot \rho_S \cdot V_{i,j,k}} \cdot R^{(0)} \tag{4.2}$$

$$I_{i,j,k}^{(2)} = I_{i,j,k}^{(0)} - \alpha_2 \cdot \frac{\Delta t}{c_S \cdot \rho_S \cdot V_{i,j,k}} \cdot R^{(1)} \tag{4.3}$$

$$I_{i,j,k}^{(3)} = I_{i,j,k}^{(0)} - \alpha_3 \cdot \frac{\Delta t}{c_S \cdot \rho_S \cdot V_{i,j,k}} \cdot R^{(2)} \tag{4.4}$$

$$I_{i,j,k}^{(4)} = I_{i,j,k}^{(0)} - \alpha_4 \cdot \frac{\Delta t}{c_S \cdot \rho_S \cdot V_{i,j,k}} \cdot \left(\frac{R^{(0)} + 2 \cdot R^{(1)} + 2 \cdot R^{(2)} + R^{(3)}}{6} \right) \tag{4.5}$$

$$I_{i,j,k}^{(n+1)} = I_{i,j,k}^{(4)} \tag{4.6}$$

with $\alpha_1 = 1/2$, $\alpha_2 = 1/2$, $\alpha_3 = 1$ and $\alpha_4 = 1$

The time-step duration Δt must be chosen very carefully. Large time-steps are preferable, but in the case of an explicit solution scheme, excessive large time-steps will result in numerical instabilities. The smaller the finite volume cells, the smaller the time-steps have to be, because of the decreasing time, which an information signal needs to pass through a smaller single cell.

5. Definition of the screw geometry as a solid domain

The screw, which will be investigated in this paper, has two threads, which means that there are existing twice as much chambers per a definite length comparing to a screw with only one thread. As a consequence of this, two opening chambers can be observed per screw rotation. The main parameter values of the geometry, which can be seen below in figure 5.1, are listed in table 5.1.

Description	Symbol	Value	Unit
Outer screw diameter	d_{outer}	0.100	m
Shaft diameter	d_{shaft}	0.040	m
Number of threads	N	2	---
Number of chambers	noc	5 *)	---
Thread pitch	h_{screw}	0.050	m
Depth of the perimeter gap	b_{PG}	0.0125	m
Width of the chambers	b_{cha}	0.0125	m
Depth of the chambers	t_{cha}	0.015	m

Table 5.1 : Main geometry parameter of the screw

*) 1 chamber with connection to the inlet / 3 closed chambers / 1 chamber with connection to the outlet

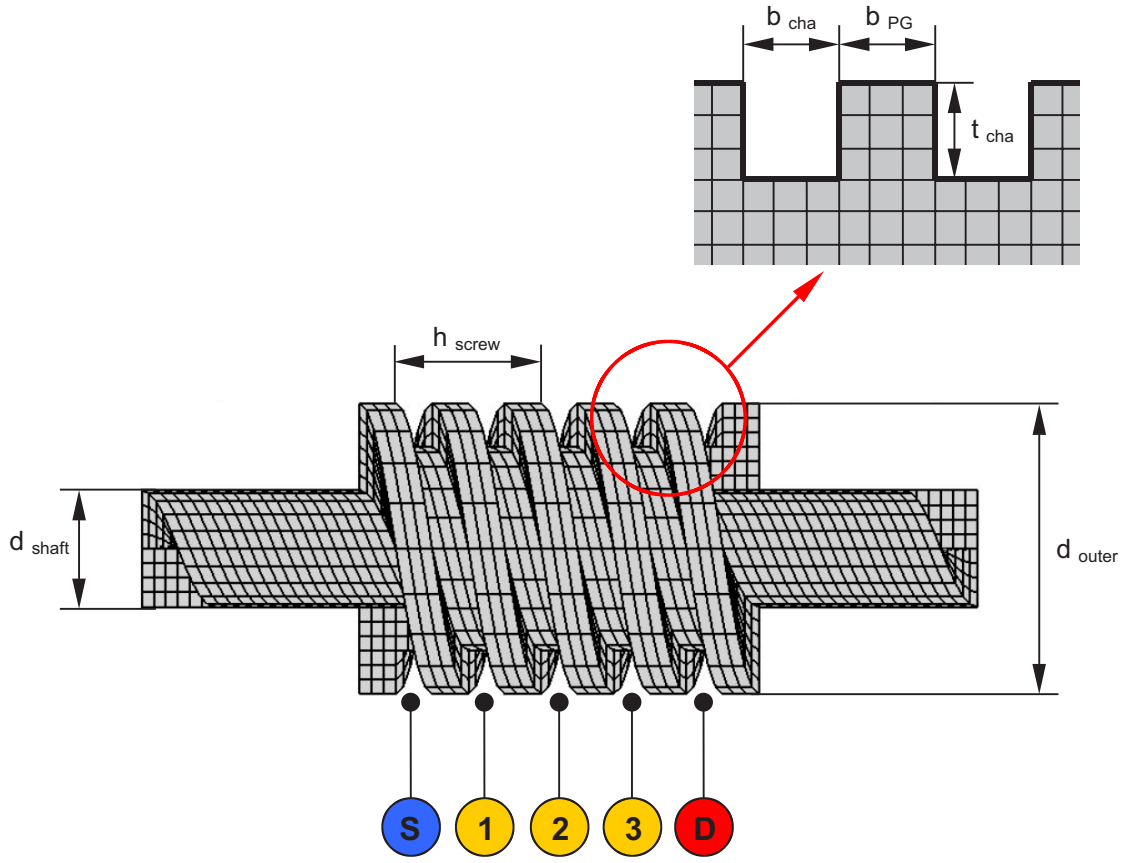

Figure 5.1 : Single screw with geometry definitions

6. Boundary conditions

To define all heat fluxes through the six cell faces everywhere inside the domain, the node temperatures of all surrounding neighbour cells have to be known. For the cells, which are describing the surface of the screw, either the temperature gradient normal to the surface or a heat flux has to be defined. This is done by the application of boundary conditions around the screw surface.

As an example, figure 6.1 shows the right end surface in the positive x-direction, two real or body cells, which are lying inside the screw and one virtual or dummy cell for the application of the boundary conditions.

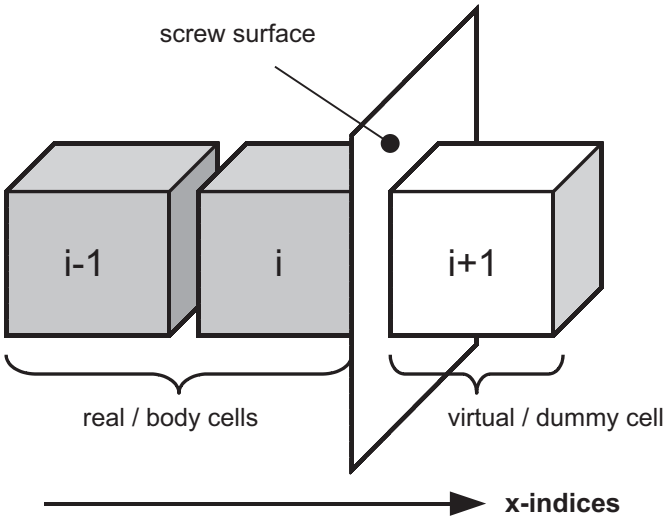

Figure 6.1 : Screw surface with adjacent cells

For the rotating screw, two kinds of thermal boundary conditions have to be distinguished. This is firstly the adiabatic wall and secondly the surface with forced convection. The correct extrapolation of the interior node temperatures to the virtual cells is explained in the figure 6.2.

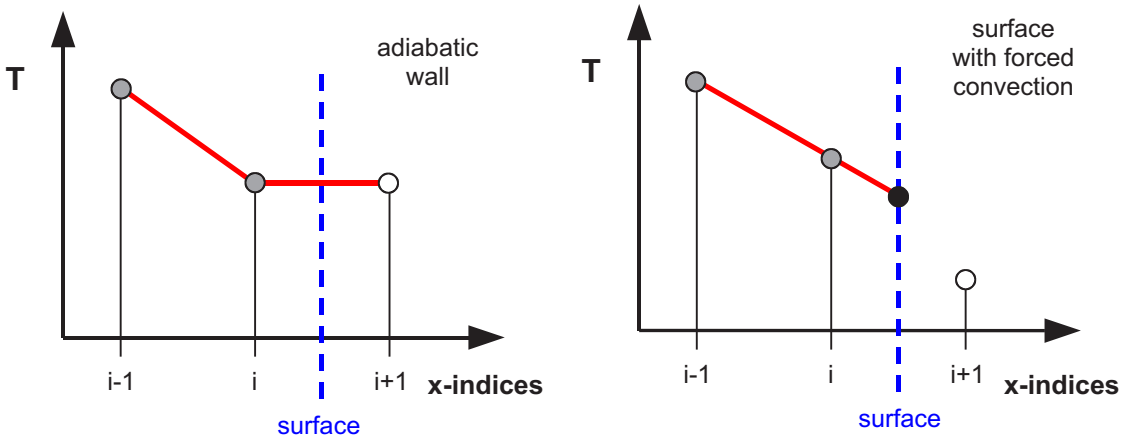

Figure 6.2 : Two kinds of thermal boundary conditions

Equation for the corresponding heat flux density of the adiabatic wall:

$$T_{i+1} = T_i \tag{6.1}$$

$$\dot{q}_{conduction} = -k \cdot \frac{\partial T}{\partial x} \tag{6.2}$$

$$\dot{q}_{conduction} = -k \cdot \frac{T_{i+1} - T_i}{x_{i+1} - x_i} = 0 \tag{6.3}$$

Equation for the corresponding heat flux density of the surface with forced convection:

$$T_{i+1} = T_\infty = T_{fluid} \tag{6.4}$$

$$T_{surface} = T_i + \frac{T_i - T_{i-1}}{x_i - x_{i-1}} \cdot 1/2 \cdot \left(x_{i+1} - x_i\right) \tag{6.5}$$

$$\dot{q}_{convection} = -h \cdot \left(T_{i+1} - T_{surface}\right) \tag{6.6}$$

The faces of all cells were forced convection is assumed are illustrated in figure 6.3, whereas the different colours stand for the three coordinate directions.

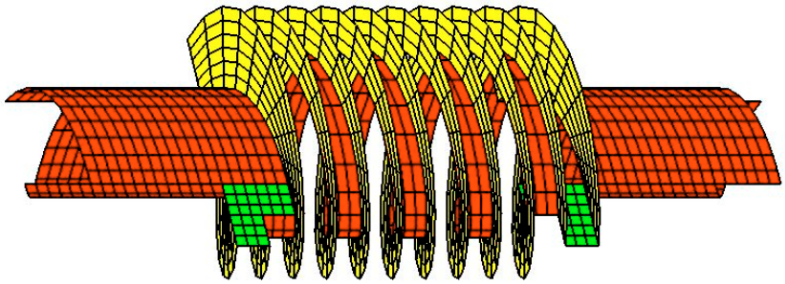

Figure 6.3 : Convective heat transfer surfaces

The most important task during the application of the different boundary condition is the correct determination of the convective heat transfer coefficients as a function of the positions of the corresponding cell faces relative to the axis of rotation. These heat transfer coefficients can be calculated by the procedure, which was explained in section 2, if the fluid conditions and properties, see table 6.1 and 6.2 around the screw are known. The results for a rotational speed of the screws of 3000 rpm are presented in table 6.3.

Position	---	S	1	2	3	4	5	D	---
Temperature	T	300	300	325	350	375	400	400	K
Pressure	p	1.0	1.0	11.0	21.0	31.0	41.0	41.0	bar
GVF	α	0.98	0.98	0.97	0.96	0.95	0.94	0.94	---

Table 6.1 : Fluid condition in the inlet, the chambers and the outlet (showcase values)

	Description	Symbol	Value	Unit
Liquid	Density	ρ_L	1000	kg / m^3
	Dynamic viscosity	μ_L	$1000 \cdot 10^{-6}$	Pa s
	Thermal conductivity	k_L	$600 \cdot 10^{-3}$	W / (m K)
	Specific heat capacity	c_L	4200	J / (kg K)
Gas	Dynamic viscosity	μ_G	$20 \cdot 10^{-6}$	Pa s
	Thermal conductivity	k_G	$25 \cdot 10^{-3}$	W / (m K)
	Isobar specific heat capacity	$c_{p\,G}$	1004	J / (kg K)
	Individual gas constant	R	287	J / (kg K)
Solid	Density	ρ_S	7850	kg / m^3
	Thermal conductivity	k_S	55	W / (m K)
	Specific heat capacity	c_S	465	J / (kg K)
	Thermal expansion coefficient	α	$12 \cdot 10^{-6}$	1 / K

Table 6.2 : Properties of the liquid / gaseous phase and the solid body

Convective heat transfer coefficients							
Position	---	1	2	3	4	5	---
Chamber flanks - min	$h_{CF\,min}$	643.2	1027.2	1357.1	1656.9	1937.0	W / (m^2 K)
Chamber flanks - max	$h_{CF\,max}$	741.1	1183.6	1563.6	1909.1	2231.8	W / (m^2 K)
Chamber grounds	h_{CG}	617.1	985.7	1302.1	1589.8	1858.5	W / (m^2 K)
Shaft surface - inlet	$h_{shaft\,in}$	441.4					W / (m^2 K)
Shaft surface - outlet	$h_{shaft\,out}$	1329.3					W / (m^2 K)

Table 6.3 : Convective heat transfer coefficients inside the chambers and on the shafts

7. Thermal expansions and their influence on the gap shapes

As a consequence of the convective heat fluxes from the surrounding fluid into the solid domain, the screw will expand accordingly to the temperature distribution inside. The perimeter gaps between the screws and the housing and the radial and flank gaps between the counter-rotating screws are rather small with a mean gap height from approximately 50 to 200 micrometers. Depending on the outer radius of the screws, a temperature increase of 100 K will already result in an unacceptable thermal expansion with an impending solid body contact between the screws or between the screws and the housing, which is assumed as stiff in this case.

The thermal expansion will be formulated here as a 2-dimensional problem in the radial and the peripheral direction, to evaluate the influence of the changing screw shape on the most important perimeter and radial gaps. In the case of the flank gap, mainly the expansions of the screw flights in the screw length direction have to be determined. The successive calculation of the 2-dimensional thermal expansion of each cell from the axis of rotation back to the screw surface follows for the lower North-West node as an example to:

For the first cell close to the axis of rotation

$$NW_{new\,i,j,k} = \begin{bmatrix} NW_{1,i,j,k} + \alpha \cdot \left(NW_{1,i,j,k} - NE_{1,i,j,k}\right) \cdot \left(T_{i,j,k} - T_{IC}\right) \\ NW_{2,i,j,k} + \alpha \cdot \left(NW_{2,i,j,k} - NE_{2,i,j,k}\right) \cdot \left(T_{i,j,k} - T_{IC}\right) \\ NW_{3,i,j,k} \end{bmatrix} \tag{7.1}$$

For each following cell

$$NW_{new\,i,j,k} = \begin{bmatrix} NW_{new\,1,i+1,j,k} + \left(NW_{1,i,j,k} - NE_{1,i,j,k}\right) + \alpha \cdot \left(NW_{1,i,j,k} - NE_{1,i,j,k}\right) \cdot \left(T_{i,j,k} - T_{IC}\right) \\ NW_{new\,2,i+1,j,k} + \left(NW_{2,i,j,k} - NE_{2,i,j,k}\right) + \alpha \cdot \left(NW_{2,i,j,k} - NE_{2,i,j,k}\right) \cdot \left(T_{i,j,k} - T_{IC}\right) \\ NW_{3,i,j,k} \end{bmatrix} \tag{7.2}$$

After determining the thermal expansions, the gap height reductions or respectively the new shapes of the several gaps can be calculated. Due to the fact, that the main proportion of the leakage flows through the perimeter and the radial gap, these both types of clearances are explained in more detail.

The perimeter gap at norm conditions equals due to the large ratio between outer screw radius and the gap height to a 2-dimensional rectangular channel, whereas the radial gap can be treated as a convergent-divergent nozzle with two different radii at the lower and the upper side, corresponding to the outer radius of the screw flight and the radius of the chamber ground. The thermal expansions of the screw and so the gap height reductions increase towards the pump discharge. From a qualitative point of view, the thermal expansions inside these two kind of gaps are presented by figure 7.1.

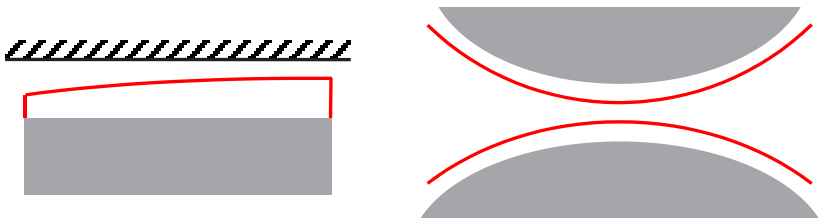

Figure 7.1 : Shape of the perimeter (left) and the radial gap (right), before (grey) and after (red) thermal expansion

Concerning the radial gap, there are two expansions in two different planes - firstly in the cross section, which can be seen in figure 7.1 and secondly perpendicular to the latter section in the screw length direction, like in the case of the perimeter gap. After the determination of the new gap shape, every gap has to be treated with a varying boundary wall to calculate the leakage flow more accurately by an additional leakage flow model.

8. Simulation results

The test case for this heat transfer model was the heat build-up of the screw with the boundary conditions explained above in section 6 and the overall initial temperature of 300 K. The simulation was accomplished with time-step duration of 0.03 seconds and was stopped after 6000 iterations or 180 seconds. The computational grid was defined by 10 cells in radial (x) direction, 20 cells in peripheral (y) direction and 69 cells in screw length (z) direction, whereas the parameter control point for example for the time history plot has the coordinates (6 / 11 / 36) in the x-y-z cell-index notation.

The time history and the residual of the temperature can be seen in figure 8.1. The simulation shows a good convergence behaviour, because of the continuous decreasing residual. In the ideal case it becomes zero, whereas the temperature time history will result in a steady state condition.

The figures 8.2 and 8.3 present two sets of temperature contour plots, which are equal to 8 cuts from the center of the screw to the outer radius over the whole screw length with an increasing peripheral angle from 9° to 171° and from 189° to 351°. The chambers with the numbers 1 to 4 (figure 8.2) and 2 to 5 (figure 8.3) can be seen as small rectangular pockets with constant temperature values at the left side of a single contour plot. The inlet and outlet region with the corresponding temperature are defined by the lower and upper large rectangular fields, which are lying also at the left side in these plots.

The next set of temperature contour plots, see figure 8.4, shows the temperature distributions in the z-y and in the y-x plane, which contain both the parameter control point. The first plot is the winding off in the peripheral direction with the constant x-value of the parameter control point. The second contour plot, represents the temperature inside the middle chamber No. 3 (see also table 6.1) and the solid material below this chamber from the chamber ground to the screw axis.

Figure 8.5 shows the temperature distribution in the cross section, which include the axis of rotation in the middle of the plot. The right subplot combines the actual temperature plot with the screw shape after the thermal expansion, but for a better visualisation with a 200-times magnified value of expansion. The colour of contours has no specified correlation with fixed temperatures, but they define a step-wise transition from the maximum possible temperature (red colour faces) to the minimum possible temperature (blue coloured faces) in the whole solid domain, which are mostly equal to the discharge and suction fluid temperature in the steady state case for example.

The figure 8.6 is similar to the previous plot, but presents the 3-dimensional screw and the temperature distribution on the screw surface. Looking at a single subplot, it can be seen, that there are existing in each case 4 chambers left and right from the screw axis. The lowest chamber of the left side is still connected with the inlet, whereas the highest chamber of the right side is already connected with the outlet. The remaining 3 chambers on each side represent the closed chambers, whereas a chamber part for example of the right side belongs to the next but one on the left side and so on. The reasons for this are on the one side the 2 screw threads and on the other side the fact, that the counter-rotating screw meshes into the visible screw from the side of observation and disconnect the apparently continuous chambers.

For a more convenient comparison between the initial screw shape and the expanded screw, figure 8.7 shows both situations in two single subplots. This was shown firstly in the cross section and secondly in the view of the 3-dimensional screw surface.

Finally it has to be said, that due to the rotation of the screw, the presented temperature distribution is just a snapshot of an exclusive screw position. To include the rotational effect, the boundary conditions or the thermodynamic and fluid dynamic chamber values have to be applied around the whole screw in peripheral direction as a function of time with the rotational speed as the main parameter.

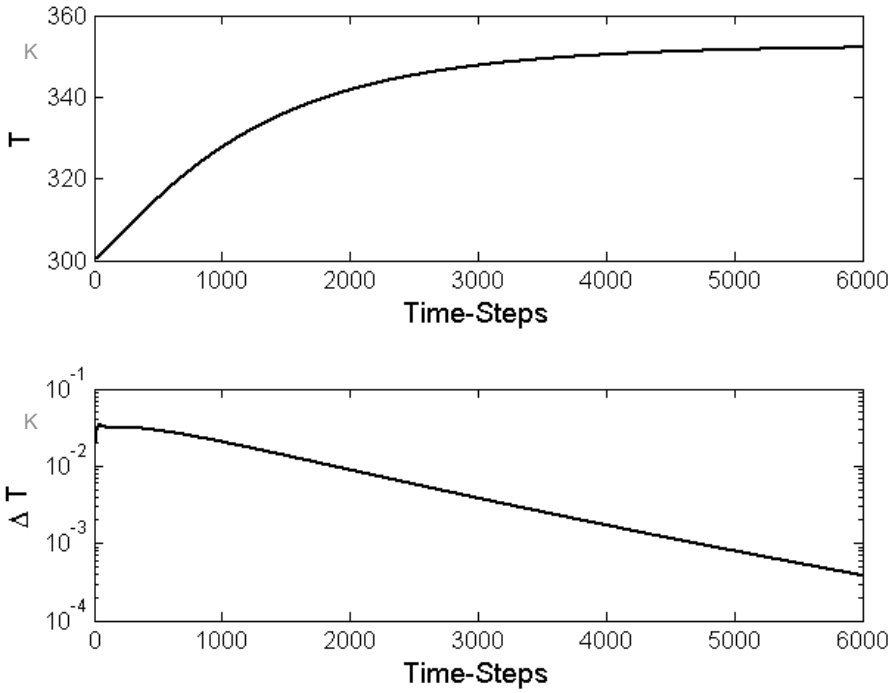

Figure 8.1 : Temperature time history and the residual as a function of time-steps

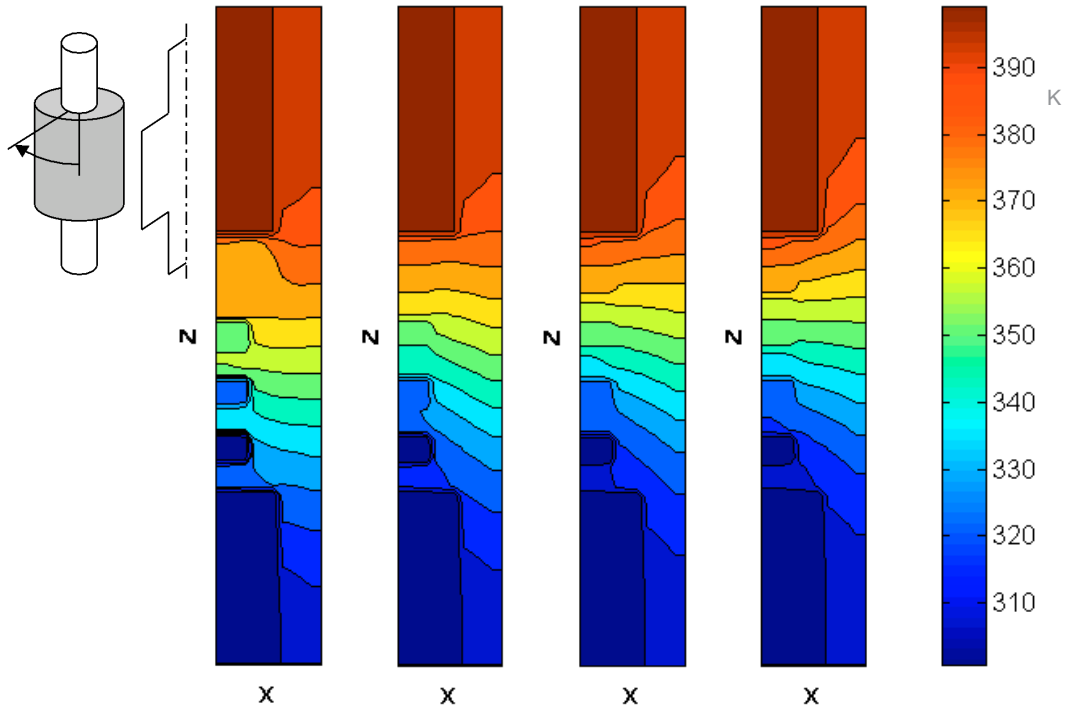

Figure 8.2 : Set of temperature contour plots (from 9° to 171° , x : radial direction , z : screw length direction)

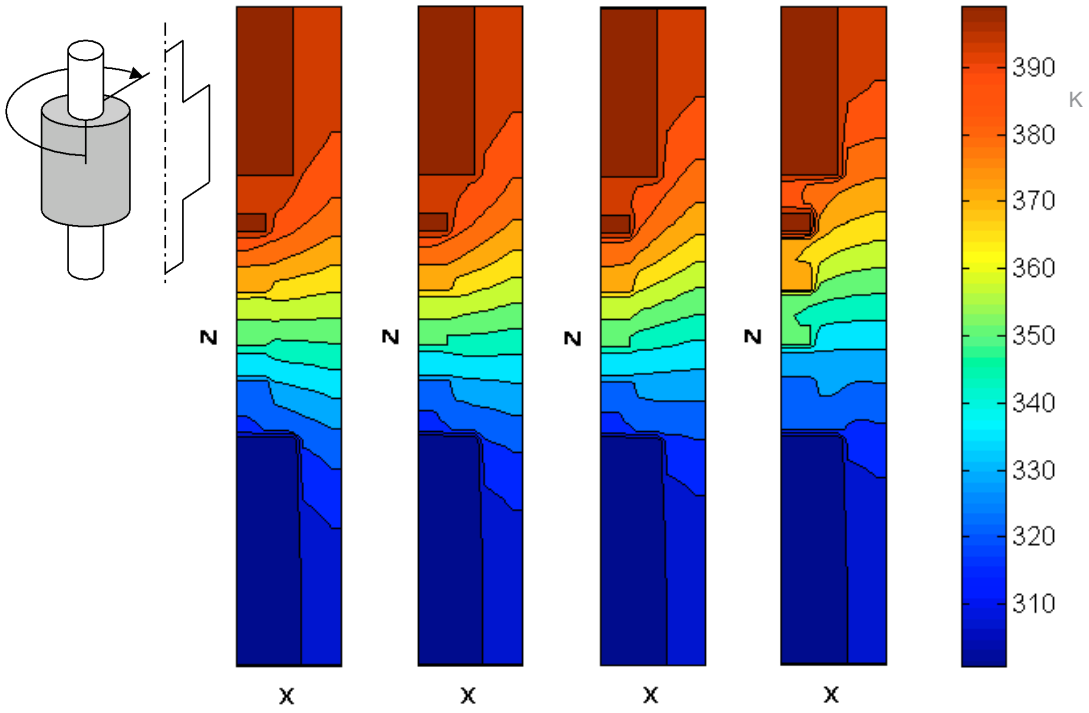

Figure 8.3 : Set of temperature contour plots (from 189° to 351° , x : radial direction , z : screw length direction)

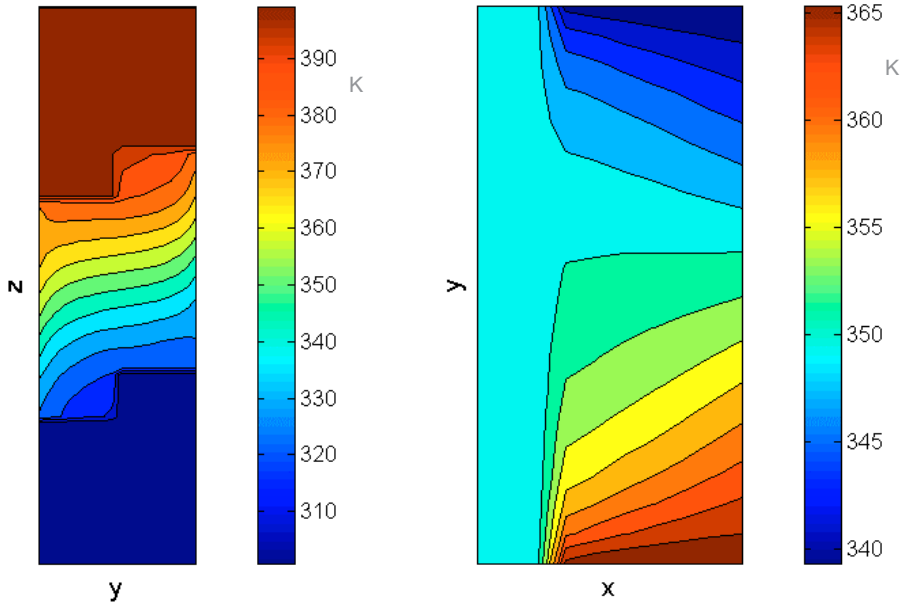

Figure 8.4 : Set of temperature contour plots (x : radial direction , y : peripheral direction , z : screw length direction)

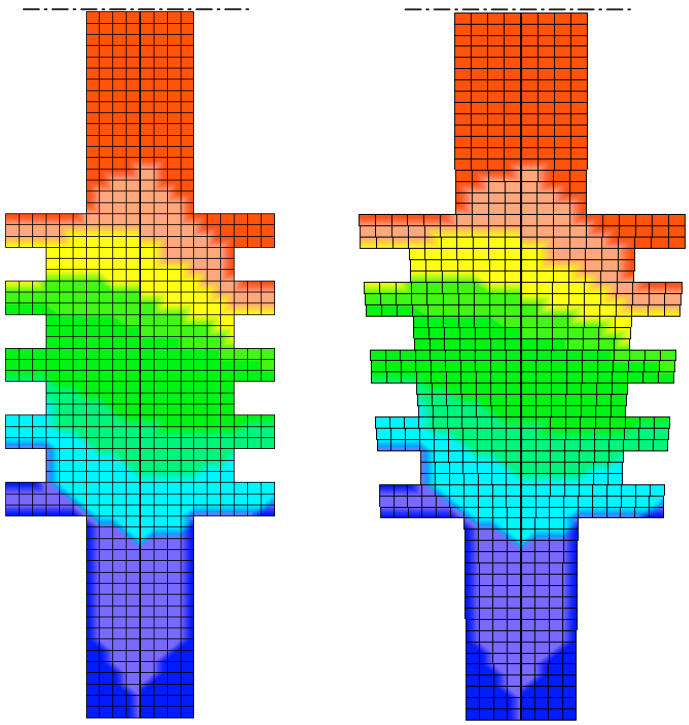

Figure 8.5 : Temperature distribution inside the screw (without and with thermal expansion)

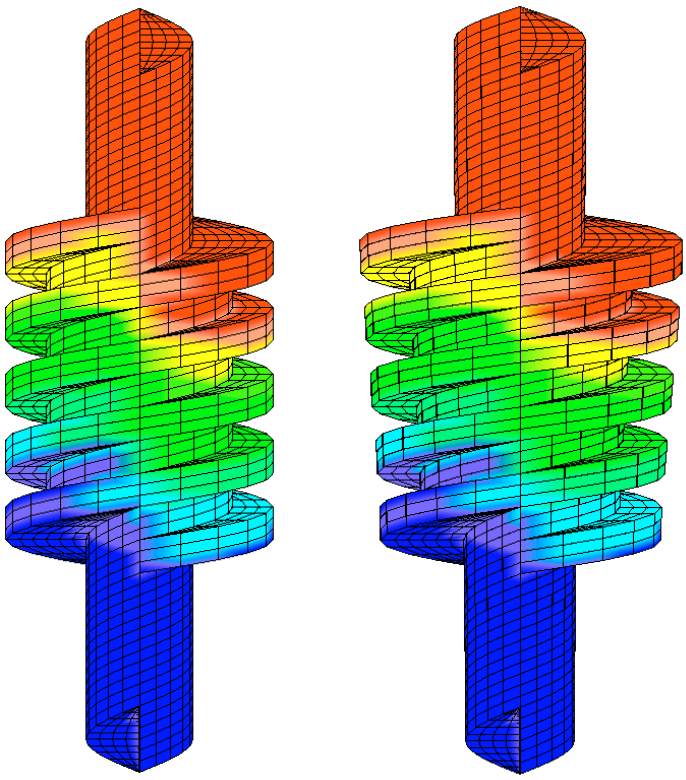

Figure 8.6 : Temperature distribution on the screw surface (without and with thermal expansion)

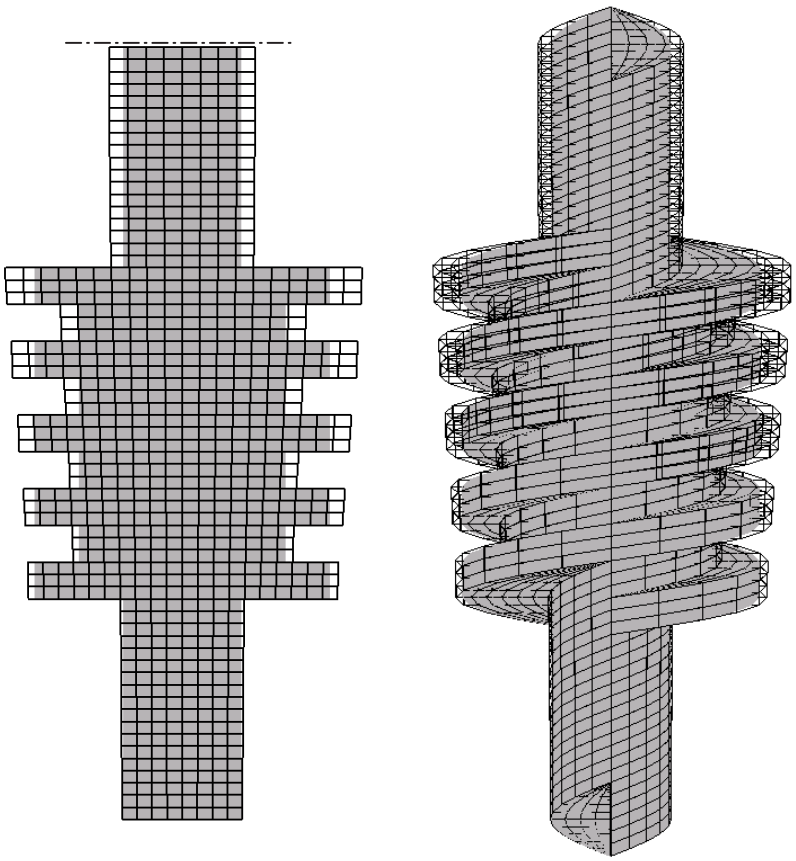

Figure 8.7 : Screw shape shifting as a result of thermal expansions

9. Conclusion

The finite volume heat transfer model, which was described in this paper, is capable of calculating the 3-dimensional heat conduction inside the screw and the convection inside the chambers and on the shaft surfaces at the suction and the discharge side of the pump. Due to the time-dependency of the calculation method, it is possible to simulate the thermal steady state and the corresponding solid expansion with the current fluid and flow condition around the screw and to determine the maximum acceptable time-span of pumping, at a point of operation, where a long-time run is not possible as a result of critical high temperature values in the chambers and the outlet. The model also gives information about the variation of the gap heights as a function of the gap length direction, which can be used in a leakage flow model to predict the mass flow more accurately. But for this step, the discretisation of the flight has to be refined, to avoid sharp discontinuities in the gap height derivative. Furthermore, the position of the first contact between the screw and the housing, which is assumed as stiff compared to the screw, and the region of a increased amount of wear can be also determined. As such the heat transfer model used in this investigation can be beneficial in the development and operation diagnostics of multiphase screw pumps.

Acknowledgements

The authors would like to thank the company LEISTRITZ for all the information about multiphase screw pumps and their additional technical support and also the Department of Mechanical and Utility Engineering of the University of Applied Sciences in Nuremberg for the computational assistance.

Nomenclature

General symbols

a	thermal diffusivity
A	area (general)
b	depth, width
c	specific heat capacity
d	diameter
D	discharge
E, N, S, W	cardinal points : east, north, south and west (node)
h	convection heat transfer coefficient; thread pitch
I	transient term, which is differentiated with respect to t
J, K, L	heat flux densities, which are differentiated with respect to x, y and z
k	thermal conductivity
L	length
m	mass
n	rotational speed
N	number of threads
p	static pressure
q	specific heat energy
Q	heat energy
r	radius
R	gas constant; term of variable changes in the Runge-Kutta scheme
S	suction
t	time; depth
T	temperature (general)
u	velocity
V	volume (general)
x	mass fraction
x, y, z	coordinates

Vectors / Matrices

A	normal vector * cell face area
n	normal vector

Greek Letters

α	gas volume fraction; Runge-Kutta factor; thermal expansion coefficient
Δ	difference
μ	dynamic viscosity
ρ	density
φ	peripheral angle
ω	angular velocity

Subscripts

CF	chamber flank
CG	chamber ground
cha	chamber
G	gaseous
h	hydraulic
H	homogeneous
i, j, k	cell indicators
in	inlet
l	cell face area index
IC	initial condition
L	liquid; lower
m,n	coordinate direction index
out	outlet
p	constant pressure
PG	perimeter gap
S	solid
U	upper
∞	condition in the infinity

Superscripts

n	current time step
n+1	following time step

Abbreviations

GVF	gas volume fraction
noc	number of cells
Nu	Nusselt number
PDE	partial differential equation
Pr	Prandtl number
Re	Reynolds number
rpm	revolutions per minute

References

[1] WINCEK, M.:
Zur Berechnung des Förderverhaltens von Schraubenspindelpumpen bei der Förderung von Flüssigkeits / Gas-Gemischen, Dissertation,
Universität Erlangen-Nürnberg, 1992
(*The calculation of the conveyance behaviour of screw pumps at the conveyance of liquid/gas-mixtures, Ph.D. thesis, University of Erlangen-Nuremberg, 1992*)

[2] KÖRNER, H.:
Zum Förderverhalten von Schraubenspindelpumpen für Zweiphasengemische hohen Gasgehalts, Dissertation,
Universität Erlangen-Nürnberg, 1998
(*The conveyance behaviour of screw pumps for two-phase mixtures with high gas-volume-fractions, Ph.D. thesis, University of Erlangen-Nuremberg, 1998*)

[3] ETZOLD, S.:
Verlustanalyse von Schraubenspindelpumpen bei Mehrphasenförderung,
Dissertation, Universität Hannover, 1993
(*Leakage analysis of screw pumps during multiphase conveyance, Ph.D. thesis, University of Hanover, 1993*)

[4] RÄBIGER, K. / MAKSOUD, T.M.A. / WARD, J. / HAUSMANN, G.:
Development of a finite volume model for the compressible gap flow inside a screw pump, Series of the University of Applied Sciences Nuremberg, No. 30, 2005

[5] NAKASHIMA, C.Y. / OLIVEIRA, S. / CAETANO, E.F.:
Thermo-hydraulic model of a twin-screw multiphase pump, ASME IMECE 04, Anaheim, USA, 2004

[6] RAUSCH, T. / VAUTH, T. / BRANDT, J.U. / MEWES, D.:
A model for the delivering characteristic of multiphase pumps, 4th North American Conference on Multiphase Technology, Banff, Canada, 2004

[7] BAEHR, H. D. / STEPHAN, K.:
Wärme- und Stoffübertragung (*Heat and mass transfer*), Springer-Verlag,
Berlin / Heidelberg, 1998

[8] WAGNER, W.:
Wärmeübertragung (*Heat transfer*),
Vogel Verlag, Würzburg, 1998

[9] INCROPERA, F.P. / DEWITT, D.P.:
Fundamentals of Heat and Mass Transfer - 4th Edition,
John Wiley & Sons, Inc., 1996

[10] POLIFKE, W. / KOPITZ, J.:
Wärmeübertragung - Grundlagen, analytische und numerische Methoden (*Heat transfer - Fundamentals, analytical and numerical methods*), Pearson Studium, München, 2005

[11] OERTEL JR., H. / LAURIEN, E.:
Numerische Strömungsmechanik (*Numerical fluid mechanics*), Springer-Verlag,
Berlin / Heidelberg, 1995

[12] WENDT, J.F.:
Computational Fluid Dynamics, Springer-Verlag,
Berlin / Heidelberg, 1996